Homopolar harmonic injection and grid synchronization in distributed control systems for grid-tied intelligent power electronic blocks in 4-wire 3-phase converters

Carlos Gómez-Aleixandre, Geber Villa, Pablo García, Andrés Suárez-González and Ángel Navarro-Rodríguez

Dept. of Electrical, Electronics, Systems & Computers Engineering

University of Oviedo, LEMUR Group, Gijón, 33204, Spain

Email: gomeztcarlos@uniovi.es, villageber@uniovi.es, garciafpablo@uniovi.es, suarezandres@uniovi.es, navarroangel@uniovi.es

Abstract—This paper studies two issues related with the use of distributed control for modular power converters based on the use of single-phase power units, namely intelligent Power Electronics Building Block (iPEBB) for power conversion in hybrid DC/AC microgrids. Some issues related to the distributed control are studied in this paper. Homopolar injection for PWM generation becomes more difficult, since each distributed controller calculates (and knows) only its control action. A possible solution is provided, based on the calculation of this homopolar injection by the central controller at 1 kHz. Synchronization with the grid becomes more difficult too, because each controller acts independently, without communication with the other ones (only with the central controller). Two alternatives are studied for this synchronization angle calculation: calculation in the central controller at central control frequency (1 kHz) or in each module at distributed control frequency (10 kHz).

I. Introduction

Nowadays, the appearance of microgrids [1], [2], small-scale power systems with distributed generation, usually with important penetration of renewable power sources, has led to an increase in the requirements for DSP/DSC capabilities, due to the large number of power electronic converters that a microgrid can have. Besides that, reliability, flexibility and scalability became especially interesting for these distributed applications. These requirements are driving to a change from traditional control architectures (based on a central controller) to decentralized architectures [3]. However, there are some drawbacks that make the implementation more difficult than the one based on a central controller. For this paper, the architecture proposed in [4] is used, as its good performance was already demonstrated.

This architecture is shown in Fig. 1. A central controller, whose control frequency is 1 kHz, calculates the current references for each converter module and send them to each distributed controller. Each controller act independently of the others by using a repetitive control [5]–[7] approach. This distributed control has a higher frequency (10 kHz, 10 times central control frequency). As demonstrated in [4], repetitive control is able to control harmonics of the fundamental frequency and negative sequence created in three-phase system due to non-linear loads and unbalances.

However, this decentralized control presents some difficulties. First, the grid synchronization, studied in Section II of this paper, has some particularities due to the distributed control topology. Conventional central control uses three-phase voltage measurements to calculate the synchronization angle. In the studied topology, this can be done but at the reduced frequency of the central controller (1 kHz) compared to the 10 kHz used at the distributed control. In this paper, individual synchronization angle calculation in each module is studied and compared to the aforementioned option.

Second, homopolar injection [8] is analyzed too. Since the common homopolar injection calculation requires to know the duty cycles at each phase, it can not be calculated at the distributed control units. A solution based on the calculation of this component by the central controller is analyzed and compared to the ideal case.

The studied case for this paper will be a 4-wire 3-phase converter (behaving as a STATCOM) connected to the grid through RL filters and with different loads at the point of common coupling.

II. Grid Syncrhonization

In this section, the two grid synchronization methods are compared. First option relies on each module calculating its own synchronization angle, as in single-phase systems using a second-order generalized integrator - frequency locked loop (SOGI-FLL) [9]. Second alternative requires the central controller to calculate the angle using a double second-order
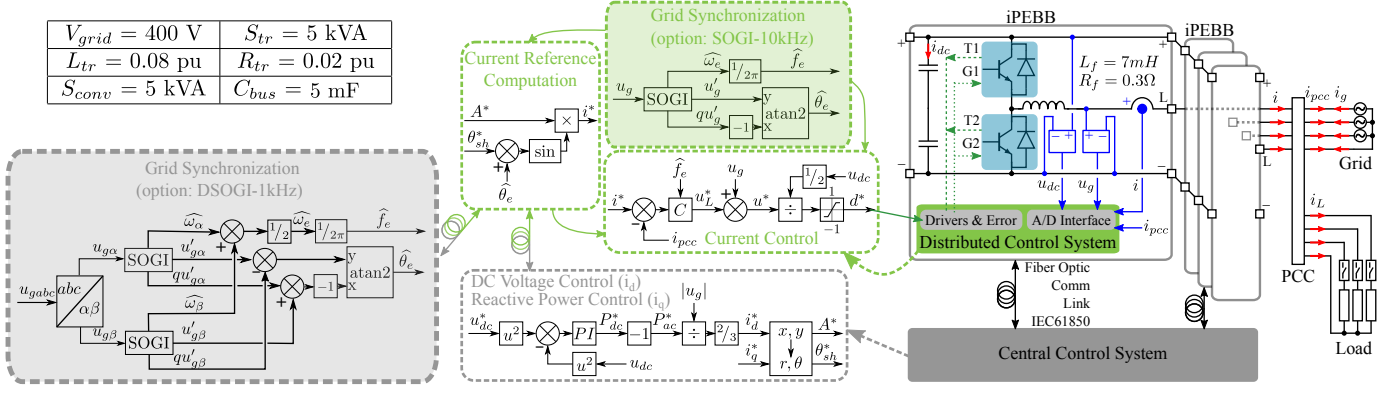
Fig. 1. System architecture proposed in [4]. Two studied alternatives for grid synchronization in shaded blocks.

generalized integrator - frequency locked loop (DSOGI-FLL) in the $\alpha\beta$ reference frame.

For the first option, sampling time will be 0.1 ms and for the second one, 1 ms. Taking this into account, a better transient response could be expected for the calculation in each distributed controller. On the other hand, the angle estimation of each distributed controller has a higher harmonic content, that could result in higher distortion of the output current. From now on, synchronization angle calculation at the central controller will be referred as central-1kHz and calculation at each distributed controller as distributed-10kHz.

A. Study case

The studied architecture is the one proposed in [4], shown in Fig. 1. Eight different cases have been simulated (when not indicated, no load at the PCC and sensors are ideal).

1) No load at the PCC and ideal sensors (ideal case).
2) At t = 0.8 s a single-phase load of rated power 75 % of per-phase rated power of the converter (1.25 kW) is connected to phase a.
3) At t = 0.8 s a three-phase load of rated power 75 % of rated power of the converter (3.75 kW) is connected.
4) At t = 0.8 s, +5 % voltage imbalance in phase a is introduced.
5) Current sensors have gain errors (+5 %, −3 %, +1 % and −2 %, for phase a, b, c and neutral).
6) Current sensors have offset errors (+0.5 A, −0.7 A, +0.2 A and +0.3 A for phase a, b, c and neutral).
7) Voltage sensors have gain errors (+3 %, −5 % and +7 %, for phase a, b and c).
8) Voltage sensors have offset errors (+10 V, −15 V and +20 V for phase a, b and c)

The initial DC link voltage is $\sqrt{2} \cdot 400$ V (approximately, the value obtained with an uncontrolled rectifier) and at t = 0.1 s the reference is set to 750 V. For the q-axis current reference, initially is set to 0 A and three change are introduced: at 0.4 s to 10 A, at 0.5 s to −10 A and at 0.6 s to 10 A.

B. Simulation results

The first simulation result to be analyzed is the angle estimation. This is shown in Fig. 2. It can be seen that
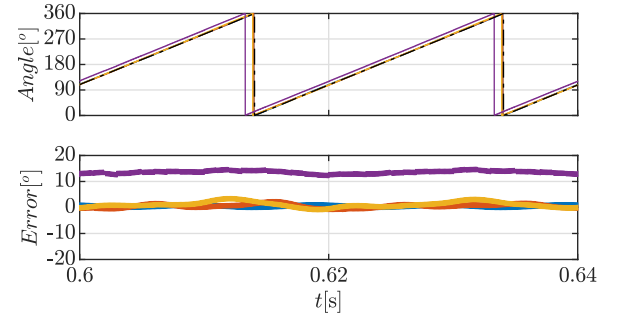

Fig. 2. Simulation results for the angle estimation. Angles for phases a, b, and c using the distributed-10kHz are represented in blue, red and yellow, whereas the central-1kHz is shown in purple. On top, the reference value (calculation at central controller at 10kHz) is depicted in black dashed line.

TABLE I
STEADY-STATE RESULTS

Case	THD (%)		i_q (A) (i_{qref} = 10 A)	
	Central	Distributed	Central	Distributed
1	0.91	1.06	10.45	9.98
2	3.13	3.44	11.11	9.92
3	5.84	1.47	10.62	9.46
4	1.6	2.08	10.43	9.97
5	0.9	0.95	9.96	9.51
6	1.43	1.12	10.44	9.96
7	2.04	1.11	10.46	9.98
8	1.97	4.56	10.45	9.84

the result in central controller estimation has an error which is approximately half of its control period, meanwhile in distributed controllers the result is really good.

The reference tracking steady state error as well as the THD for the grid current are shown in Table I. It has to be remarked that the results for the case 3 are not relevant since, as it will be shown later, its transient response for central-1kHz is too slow for the needed dynamic response in this application and the control becomes unstable when the used load is connected..

As a summary of the results presented in Table I, it can be stated that, in general, central-1kHz produces slightly lower harmonic distortion than distributed-10kHz, except for case 8 in which this difference becomes more important (offset in
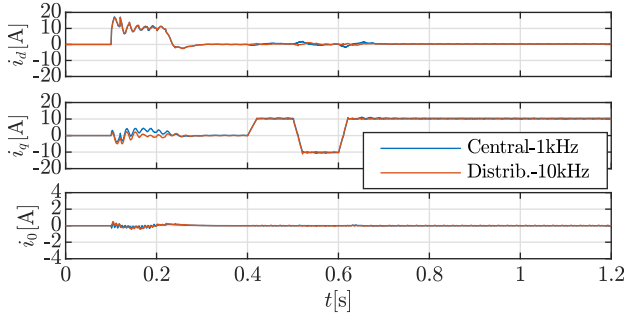
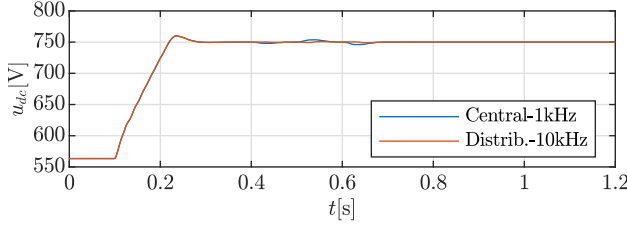Fig. 3. Simulation results for dq0 current for case 1.

Fig. 5. Simulation results for dq0 current for case 2.

Fig. 4. Simulation results for DC link voltage for case 1.

Fig. 6. Simulation results for DC link voltage for case 2.

Fig. 7. Simulation results for DC link voltage for case 3.

voltage measurement creates significant harmonic content in angle estimation using distributed implementation) and case 6 and 7 in which distributed-10kHz achieves lower distortion. This is due to the fact that since they do not have communication, angle estimation in each of three distributed controllers do not have exactly 120º phase shift. For the capability of following i_{qref}, it can be seen that the distributed controller has better performance in all the cases (neglecting case 5 and 6, which are the ones with current sensor errors) being significant in some of them (especially case 2, where central-1kHz has 11 % error and for distributed-10kHz is 0.8 %).

For the transient response analysis, the DC link voltage and the converter output currents in the $dq0$ reference frame were obtained for the different cases. Due to room constraints, only the results for cases 1, 2, 3 and 8 are included.

C. Ideal case

Starting with the ideal case shown in Fig. 3 and 4, it can be seen a very similar behavior in both cases, being slightly better in distributed-10kHz for the d-axis and q-axis components and slightly worse in the 0 component. It is important to notice that, even for this ideal case, the changes in the reactive power reference causes momentary deviations of the DC link voltage from the reference value for the central-1kHz. This is due to the errors in the estimated synchronization angle.

D. Single-phase load

In the case of the single-phase load connected at t = 0.8 s, shown in Fig. 5 and 6, the results are very similar to the previous ones. It is important to point that the controller is able to stabilize the reactive current injection even though the significant unbalance, which affects the DC link voltage
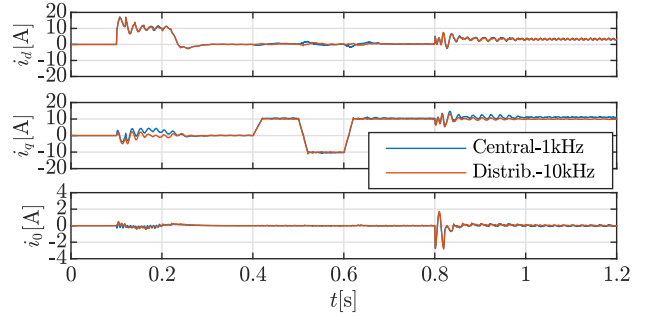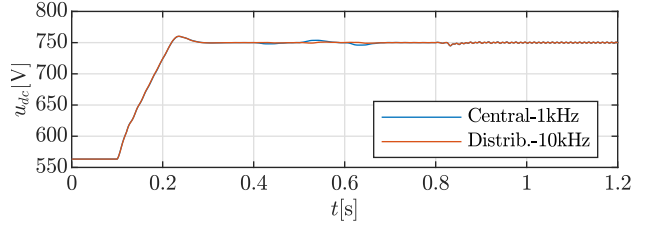
ripple. A small DC link voltage drop appears when the load is connected, but both methods are able to fast recovery.

E. Three-phase load

For the three-phase load connection at t = 0.8 s, shown in Fig. 7, a really important result is obtained. Because of the sudden introduction of a significant power demand, both systems have a noticeable DC link voltage drop, but distributed-10kHz is fast enough to recover the reference voltage meanwhile central-1kHz is too slow and the control becomes unstable.

F. Offset error in voltage sensors

Last case to be analyzed corresponds to the effect of voltage sensors offsets. Results are shown in Fig. 8 and 9. The shown results are the worst case, in terms of steady state, for distributed implementation. For transient response, the comparison between both methods is similar to the one done in the ideal case: distributed implementation follows better d-axis and q-axis current reference and both methods have similar operation regarding DC link voltage, except from moments when reactive power reference changes (deviations of DC link voltage from reference value for the central implementation).
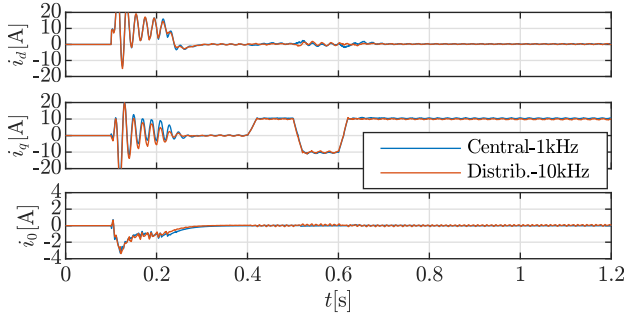
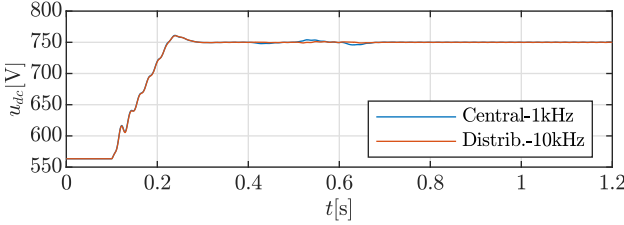Fig. 8. Simulation results for dq0 current for case 8.

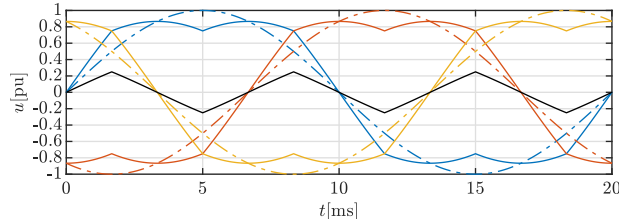Fig. 9. Simulation results for DC link voltage for case 8.

Fig. 10. Homopolar injection principle.

III. HOMOPOLAR HARMONIC INJECTION

In this section, a method for homopolar injection in the distributed system is proposed, since calculations with voltage measurements for each leg can not be done at switching frequency. Homopolar harmonic injection [8] consist on adding to the control actions of all the legs of the 3-phase system the same voltage, so that the output does not vary (phase-to-phase voltage does not change) but some extra margin is obtained. This allows to obtain higher control action outputs for the same DC link voltage. In Fig. 10, this principle is shown. As shown, homopolar harmonic injections achieves a reduction of sqrt(3/2) for the peak value (more than 13 % reduction). This is implemented by adding a triangular waveform to the three phases, which in steady state has a frequency 6 times higher than the fundamental one and a maximum value of 0.25 the sinusoidal magnitude. At each switching cycle, the magnitude can be calculated as:

$$u_{max-triangular} = 0.25\sqrt{\frac{u_a^2 + u_b^2 + u_c^2}{1.5}} \qquad (1)$$

However, at the proposed distributed control system, the information required to make the calculation, control action of all the phases (and neutral if used), is only available at
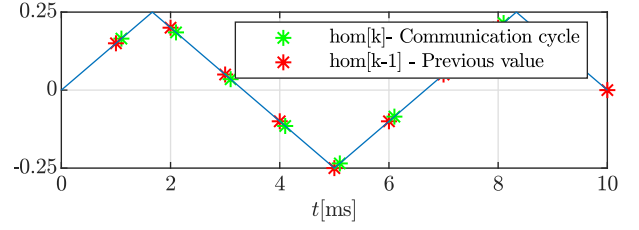

Fig. 11. Homopolar injection communication cycles.

if $n = 0$ **then** ▷ (Calculations at synchronization cycle)
$max[k] = 0.25\sqrt{\frac{u_a^2 + u_b^2 + u_c^2}{1.5}}$;
$hom[k] = -\frac{max(u_{abcn}[k]) + min(u_{abcn}[k])}{2}$;
$hom[k-1] = -\frac{max(u_{abcn}[k-1]) + min(u_{abcn}[k-1])}{2}$;
   if derivative method **then**
      $slope[k] = hom[k] - hom[k-1]$;
   end if
   if waveform estimation method **then**
      $slope[k] = 6 \cdot max[k] \cdot fe/fsw$;
   end if
else
   $hom[k+n] = hom[k] + n \cdot slope[k]$;
   if $hom[k+n] > max[k]$ **then**
      $hom[k+n] = 2 \cdot max[k] - hom[k+n]$;
   end if
   if $hom[k+n] < -max[k]$ **then**
      $hom[k+n] = -2 \cdot max[k] - hom[k+n]$;
   end if
end if

Fig. 12. Algorithm for calculation of homopolar injection. Real implementation is split in two parts. The calculations when $n = 0$ are done in the central controller (at 1 kHz) and the rest is done in each distributed controller (at 10 kHz). $slope$, slope of the triangular waveform. hom, value of the homopolar injection; $[k]$, corresponding to a communication cycle; $[k+n]$, n-th cycle after communication; max, amplitude of triangular waveform.

the central controller. As the central controller runs 10 times slower than the distributed one, the homopolar component can not be obtained at each distributed control cycle.

In this paper, two solutions for this problem are analyzed, both of them based on the calculation of the homopolar component at the central controller. For both alternatives, the central controller calculates the homopolar component corresponding to the last cycle control action of the distributed controllers and sends it back to each distributed unit. Apart from that, the method requires to know the maximum value of the homopolar injection triangular waveform and its slope.

In Fig. 11 and Fig. 12, both solutions are shown. Both use the same procedure for all calculations, but they differ in the way the slope is calculated.

The first one calculates the slope as the derivative (obtained with last two values). This method is very sensitive to values which lie outside the normal trend of the triangular waveform, since this difference is magnified each cycle (this deviation from the trend is used for calculating the derivative which is
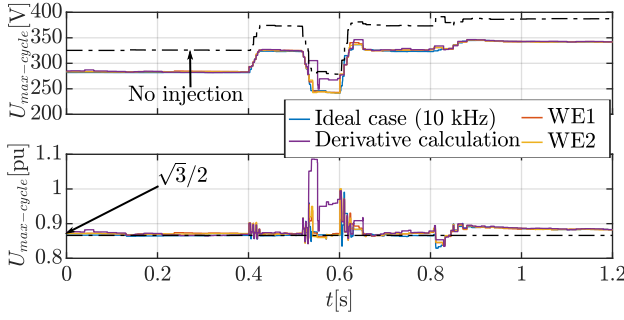
Fig. 13. Simulation results for homopolar injection (WE: waveform estimation; 1 or 2: number of used last values).

used to calculate next steps). From now on this method will be referred as derivative calculation.

Second alternative is based on an estimation of the triangular waveform since the expected characteristics (frequency and peak value) are known and the phase of the triangular waveform can be easily estimated (done by synchronization with zero-crossing detection). For minimizing the effect of values outside the normal trend of the triangular waveform, this method was tested by considering only the last measurement or last two measurements. From now on this method will be named as waveform estimation (WE, WE1 when taking into account last value and WE2 when considering lat two).

For testing the different alternatives, some simulations were carried out using Simulink/Matlab. The performance was tested by applying the different methods to the same study case, applying some steps to the q-axis current reference of the STATCOM: from 0 to 10 A at t = 0.4 s, from 10 to −10 A at t = 0.5 s and from −10 to 10 A at t = 0.6 s. At t = 0.8 s a three-phase load of rated power 75 % of rated power of the converter (3.75 kW) is connected. The initial voltage for the simulation is 750 V, which is also the reference value.

Homopolar harmonic injection allows to increase maximum converter delivered voltage by adding the same signal to the three phases and neutral legs. Since this extra voltage margin is translated to a reduction in the duty control action for the same current regulation requirements, the performance is evaluated by looking at the control action values in each leg at each switching cycle. A figure of merit is obtained by analyzing the maximum absolute value for all the legs. These results are shown in Fig. 13. First graphic presents the absolute values of the control actions and the second one as a per unit value of each method compared to the case with no injection to see how much reduction is achieved (ideally, $\sqrt{3}/2$).

The results using the derivative method have a degraded performance in certain transient responses. This is due to small deviations of one of the values from the trends produce important errors in the calculation of the following ones. Both options considering waveform estimation (with one or two previous values) obtain results close to the ideal case.

For quantifying the result, the error of all options was calculated (as the integral of the difference between the obtained value of output voltage and the reference one, $\sqrt{3}/2$)

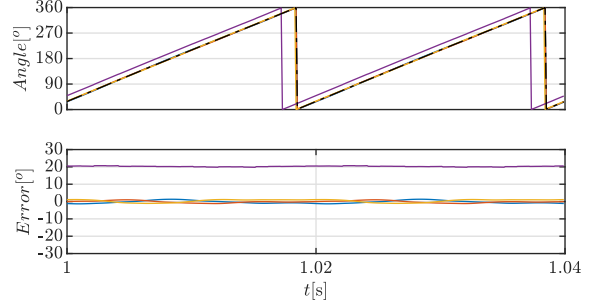| L_{filter}	7 mH	R_{filter}	0.3 Ω	C_{bus}	5 mF
V_{dc-bus}	800 V	S_{conv}	10 kVA	f_{switch}	10 kHz

Fig. 14. Experimental results for the angle estimation. Angles for the a, b, and c phases using the distributed controller are represented in blue, red and yellow, whereas the central controller estimation is shown in purple. On top, the reference value (DSOGI at 10kHz) is depicted in black dashed line.

and compared to the ideal case. The error in the derivative case is 2.25 times the one in the ideal case, meanwhile in waveform estimation is 1.41 and 1.35 times the ideal one (for one and two last values respectively).

IV. EXPERIMENTAL RESULTS

In this section, some experiments were performed to confirm the conclusions obtained from simulations tests. The topology is the one shown in Fig. 1, working during initial experimental validation in 3-wire mode. Parameters are listed in Table II.

A. Grid synchronization

For comparing the performance of both alternatives for grid synchronization (angle calculation with three-phase measurement at the central controller with reduced frequency - 1 kHz - or with single-phase measurement at each distributed controller at 10 kHz) some experiments were performed.

The initial DC link voltage is $\sqrt{2}\cdot 400$ V (the value obtained with an uncontrolled rectifier) and at t = 0.2 s the reference is set to 800 V. For the q-axis current reference, initially is set to 0 A and three change are introduced: at 0.6 s to 20 A, at 0.8 s to −20 A and at 1 s to 20 A. At t = 1.2 s a three-phase load of 3.2 kW is connected.

Synchronization performance for both the central and the decentralized approaches are compared by the accuracy of the estimated grid angle. Results are shown in Fig. 14. It can be seen that the result in decentralized approach is good, having an error of less than 2 deg. However, the error in central approach is much higher and corresponds to a pure delay of a sampling time (sampling time of 1 ms over 20 ms of voltage fundamental period: $1/20 \cdot 360$ deg. = 18 deg.).

Fig. 15 shows the output current using both methods. As it can be seen, the results are slightly better in the case of distributed-10kHz. The shown ripple probably comes from aliasing (main harmonic components in both methods appear at −100 and 100 Hz).
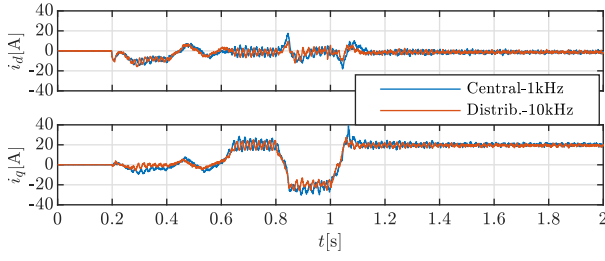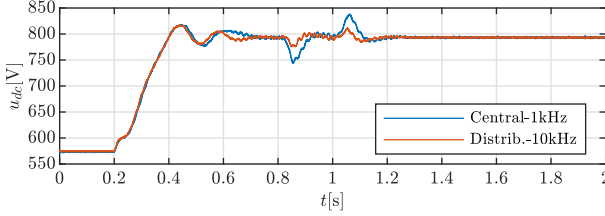
Fig. 15. Experimental results for dq current.

Fig. 16. Experimental results for DC link voltage.

Fig. 17. Experimental results for homopolar injection (WE: waveform estimation; 1 or 2: number of used last values).

The steady-state response has been evaluated using the THD obtained with both methods. The obtained results are very similar in both cases, 5.94% for the distributed-10kHz 6.00 % for the central-1kHz.

In Fig. 16, DC link voltage is shown. As it can be seen, also matching the simulation results, there is a significant difference in terms of DC link voltage control. The faster response of angle estimation using the distributed-10kHz achieves a much better behavior (even though the angle is estimated by using only single-phase measurements).

B. Homopolar injection

For the experimental validation, a similar test to the one performed in simulations was done. Changes in the STATCOM q-axis current reference were sequentially commanded as follows: from 0 to 20 A at t = 0.8 s, from 20 to −20 A at t = 1 s and from −20 to 20 A at t = 1.2 s.

The evaluation of homopolar harmonic injection performance was done using the same procedure than the one used in simulation. The results are shown in Fig. 17. The error in the derivative case is 1.82 times the one in the ideal case, meanwhile, using the waveform estimation it is reduced to 1.70 and 1.68 times the ideal one for the alternatives using one one and two last values respectively).

V. CONCLUSIONS

This paper has analyzed two drawbacks when using distributed control systems for the control of multi-phase power converters in dc/ac microgrids. First, the grid-synchronization has been tackled. The operation for the two proposed methods is similar in terms of steady-state result for angle calculation. However, in terms of transient response, the overall response is much better in the case of angle calculation in each distributed controller, especially regarding DC link voltage control. Taking this into account, the proposed solution is
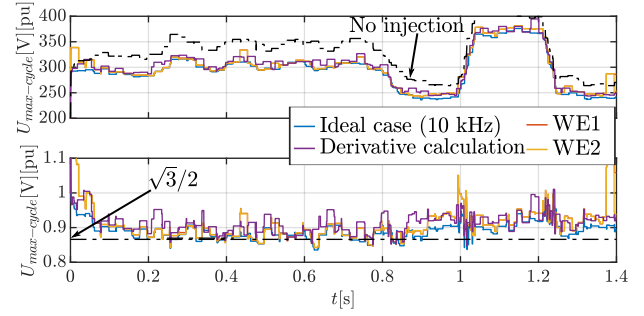
clear and the calculation of the synchronization angle by each distributed controller is chosen.

Second, different alternatives for homopolar harmonic injection were tested both in simulations and experiments. The method based on the estimation of the waveform taking into account its triangular waveform was proved to give a good performance. It has relatively similar result when compared to the ideal case (homopolar injection calculated at switching frequency) and better than the one obtained by using the derivative approach. No important differences between the method using one or two previous values is obtained, still, slight better results are obtained with two.

As focus of actual research, the effects of communications (delays or data loss) for both synchronization and homopolar injection should be assessed.

REFERENCES

[1] J. M. Guerrero, P. C. Loh, T. Lee, and M. Chandorkar, "Advanced control architectures for intelligent microgridspart ii: Power quality, energy storage, and ac/dc microgrids," *IEEE Transactions on Industrial Electronics*, vol. 60, no. 4, pp. 1263–1270, April 2013.

[2] P. Wang, X. Liu, C. Jin, P. Loh, and F. Choo, "A hybrid ac/dc micro-grid architecture, operation and control," in *2011 IEEE Power and Energy Society General Meeting*, July 2011, pp. 1–8.

[3] R. Pea-Alzola, G. Gohil, L. Mathe, M. Liserre, and F. Blaabjerg, "Review of modular power converters solutions for smart transformer in distribution system," in *2013 IEEE Energy Conversion Congress and Exposition*, Sep. 2013, pp. 380–387.

[4] G. Villa, C. Gómez-Aleixandre, P. García, and J. García, "Distributed control alternatives of modular power converters for hybrid dc/ac microgrids," in *2018 IEEE Energy Conversion Congress and Exposition (ECCE)*, Sep. 2018, pp. 6379–6386.

[5] S. Hara, Y. Yamamoto, T. Omata, and M. Nakano, "Repetitive control system: a new type servo system for periodic exogenous signals," *IEEE Transactions on Automatic Control*, vol. 33, no. 7, pp. 659–668, Jul 1988.

[6] M. Tomizuka, T. C. Tsao, and K. K. Chew, "Discrete-time domain analysis and synthesis of repetitive controllers," in *1988 American Control Conference*, June 1988, pp. 860–866.

[7] A. Lidozzi, C. Ji, L. Solero, F. Crescimbini, and P. Zanchetta, "Load-adaptive zero-phase-shift direct repetitive control for stand-alone four-leg vsi," *IEEE Transactions on Industry Applications*, vol. 52, no. 6, pp. 4899–4908, Nov 2016.

[8] F. Briz, A. Diez, M. W. Degner, and R. D. Lorenz, "Current and flux regulation in field-weakening operation [of induction motors]," *IEEE Transactions on Industry Applications*, vol. 37, no. 1, pp. 42–50, Jan 2001.

[9] M. L. Remus Teodorescu and P. Rodriguez, *Grid Converters for Photovoltaic and Wind Power Systems*. John Wiley-IEEE, 2011.